3832–3847 *Nucleic Acids Research, 2020, Vol. 48, No. 7* *Published online 7 February 2020*
doi: 10.1093/nar/gkaa052

RNA processing machineries in Archaea: the 5′-3′ exoribonuclease aRNase J of the β-CASP family is engaged specifically with the helicase ASH-Ski2 and the 3′-5′ exoribonucleolytic RNA exosome machinery

Duy Khanh Phung[1,†], Clarisse Etienne[1,†], Manon Batista[1], Petra Langendijk-Genevaux[1], Yann Moalic[2], Sébastien Laurent[2], Sophie Liuu[3], Violette Morales[1], Mohamed Jebbar[2], Gwennaele Fichant[1], Marie Bouvier[1], Didier Flament[2] and Béatrice Clouet-d'Orval[1,*]

[1]Laboratoire de Microbiologie et de Génétique Moléculaires, UMR5100, Centre de Biologie Intégrative (CBI), Université de Toulouse, CNRS, Université Paul Sabatier, F-31062 Toulouse, France, [2]Ifremer, Univ Brest, CNRS, Laboratoire de Microbiologie des Environnements Extrêmes, F-29280 Plouzané, France and [3]Micalis Institute, PAPPSO, INRA, AgroParisTech, Université Paris-Saclay, 78350, Jouy-en-Josas, France

Received October 24, 2019; Revised January 14, 2020; Editorial Decision January 16, 2020; Accepted January 23, 2020

ABSTRACT

A network of RNA helicases, endoribonucleases and exoribonucleases regulates the quantity and quality of cellular RNAs. To date, mechanistic studies focussed on bacterial and eukaryal systems due to the challenge of identifying the main drivers of RNA decay and processing in Archaea. Here, our data support that aRNase J, a 5′-3′ exoribonuclease of the β-CASP family conserved in Euryarchaeota, engages specifically with a Ski2-like helicase and the RNA exosome to potentially exert control over RNA surveillance, at the vicinity of the ribosome. Proteomic landscapes and direct protein–protein interaction analyses, strengthened by comprehensive phylogenomic studies demonstrated that aRNase J interplay with ASH-Ski2 and a cap exosome subunit. Finally, *Thermococcus barophilus* whole-cell extract fractionation experiments provide evidences that an aRNase J/ASH-Ski2 complex might exist *in vivo* and hint at an association of aRNase J with the ribosome that is emphasised in absence of ASH-Ski2. Whilst aRNase J homologues are found among bacteria, the RNA exosome and the Ski2-like RNA helicase have eukaryotic homologues, underlining the mosaic aspect of archaeal RNA machines. Altogether, these results suggest a fundamental role of β-CASP RNase/helicase complex in archaeal RNA metabolism.

INTRODUCTION

Post-transcriptional regulation of gene expression demands accurate and timely RNA processing and decay to ensure coordinated cellular behaviours and fate decisions. Therefore, understanding RNA metabolic pathways and identifying RNA processing machineries, composed in general of ribonucleases (RNases) and ancillary enzymes such as RNA helicases, are major challenges in RNA biology. Currently, the best-understood RNA-dedicated pathways at the molecular level are those of Bacteria and Eukarya. In contrast, in Archaea, these molecular processes have been overlooked and are far from being understood.

Archaea, micro-organisms with signature sequences reported in all terrestrial and in human microbiome (1), have attracted considerable attention because of the orthologous relationships existing between their information processing machineries and those of eukaryotes (2–8). Regarding RNA machineries, it is worth mentioning that the archaeal 70S ribosome appears to be a simplified orthologous version of the eukaryal 80S ribosome with a reduced protein number (9,10) and that the archaeal RNA polymerase (RNAP) shares several features with eukaryal RNAPII such as similarities in amino acid sequences and of structures (11,12). Furthermore, most archaeal genomes contain genes encoding an evolutionary-conserved phosphorolytic 3′-5′ RNA-degrading machinery, the RNA exosome (13), with the exception of Halophiles and some methanogens that possess homologues of bacterial RNase R (14,15). In addition to its ribonucleolytic activity, the archaeal RNA exosome possesses a 3′-end RNA-tailing activity (14). This machinery,

*To whom correspondence should be addressed. Tel: +33 561 335 875; Fax: +33 561 335 886; Email: Beatrice.Clouet-dOrval@ibcg.biotoul.fr
†The authors wish it to be known that, in their opinion, the first two authors should be regarded as Joint First Authors.
Present address: Duy Khanh Phung, University College London, Gower Street, Darwin Building, London WC1E 6BT, UK.

which shares high sequence and structure similarity with its eukaryotic counterpart, is constituted of a central catalytic core of three dimers of Rrp41-Rrp42 forming an hexamer ring with the three Rrp41 subunits carrying the catalytic activity (16–18). On the top, an RNA-binding platform composed of a trimer of Rrp4 and/or Csl4 subunits that has high affinity for A-rich RNA sequences and that is required for effective RNA degradation form the RNA exosome cap (19–22). In addition, a protein annotated as DnaG, composed of a primase domain, is part of the RNA exosome cap through an interaction with Csl4 (23). To date, the contribution of the archaeal RNA exosome to specific biological pathways is still unknown and it remains to determine if archaeal cells harbour dedicated RNA exosomes, with heterogeneous and/or homogenous trimer cap composition *in vivo*.

The β-CASP RNases appear as versatile ancient enzymes with dual endo- and 5′-3′ exo-ribonucleolytic activities that act to control RNA maturation and stability in Bacteria and Eukarya (24,25). Our previous studies identified and characterized three major groups of archaeal β-CASP RNases: aCPSF1 and aCPSF2 orthologous to the eukaryal Cleavage & Polyadenylation Specific factor CPSF73 and aRNase J orthologous to bacterial RNase J (26). This composite setting raises the question of the role of each β-CASP group in archaeal RNA homeostasis as well as the evolutionary origin of this family of enzyme among the three domains of life. In recent highlights on this mosaic system, we proposed potential functions within RNA-degradation machineries in Archaea (15,27).

In Eukarya and Bacteria, as a general common thread, both mRNA decay and translation are intimately coordinated. These involve, after decapping/deprotection and deadenylation, the 5′-3′ exoribonucleolytic activity supplied by the eukaryal Xrn1 or bacterial RNase J exo-RNases, which is complemented by the 3′-5′ exoribonucleolytic activity supplied by the eukaryal RNA exosome or bacterial PNPase, respectively (28,29). Conserved 5′-3′ exoribonucleolytic activities are crucial in mRNA homeostasis in all eukaryotic and most bacterial cells. In archaeal cells, the 5′-3′ exoribonucleolytic activity is also conserved and is carried by aRNase J and aCPSF2. The role of this activity has been little studied (30,31) and it remains to be clarified in which specific RNA decay and processing pathways it is involved. aRNase J and aCPSF2 exo-RNases have been identified being highly processive and having a preference for mono-phosphorylated RNA substrates in Euryarchaeota and Crenarchaeota, respectively (32,33). In addition, a directional 5′-3′ RNA decay pathway was proposed to be at play in the crenarchaeal *Sulfolobus solfataricus* cells. *In vitro* and *in vivo* studies evidenced cap-like structure of translation initiation factor (aIF2-γ), protecting RNA 5′-triphosphorylated ends from a 5′-end-dependent decay (30,33–34).

In this study, we focus on aRNase J as we identified this enzyme to be encoded in most of the Euryarchaeota phylum (26,32,35–36). Deciphering the physiological functions and relevance of 5′-3′ ribonucleolytic activity of the aRNase J is a mandatory step towards understanding its impact on cellular RNA homeostasis in euryarchaeal cells. Using combined biochemical, proteomics and genetics coupled with phylogenomic analyses, we show that aRNase J forms a widely-conserved multi-protein complex with the archaeal specific helicase of the Ski2 family, ASH-Ski2 and we present evidences that, in Thermococcales cells, the aRNase J cross-talks with the RNA exosome. Moreover, our mutational analyses pinpoint functionally important domains involved in the aRNase J/ASH-Ski2 and aRNase J/Csl4 protein–protein interactions, respectively. Finally, we observed that a potential aRNase J–ribosome interaction exists and that could physically link 5′-3′ mRNA decay to translation in Euryarchaeota.

Altogether, our work builds the first blocks of complexes and networks involved in RNA-metabolic pathways in Euryarchaea as we propose that aRNase J participates in RNA decay routes in the vicinity of the ribosome, in coordination with the ASH-Ski2 helicase and/or the RNA exosome, pointing a close relationship between the RNA exosome and Ski2-like helicase in Euryarchaea. The mosaic setting of players around the 5′-3′ exo-RNase aRNase J, which is orthologous to bacterial RNase J, give a milestone towards the conservation of general principles of RNA-processing across the three domains of life since the ASH-Ski2 and RNA exosome have homologues found in Eukarya.

MATERIALS AND METHODS

Vectors and Oligonucleotides

The supplementary Tables S1 and 2 summarize T7-promotor-driven pET vectors and oligonucleotides used in this study. All constructions were obtained by assembling polymerase chain reaction fragments using InFusion® cloning kit (Takara). Using appropriate sets of oligonucleotides, pET vectors were amplified with the PrimeSTAR Max DNA polymerase (Takara) and the coding sequence of *Pyrococcus abyssi* aRNase J (PAB1751), ASH-Ski2 (PAB2313), Hel308 (PAB0592), DnaG (PAB0316), Rrp41 (PAB0420), Rrp4 (PAB0419) and Csl4 (PAB2314) were amplified from genomic DNA using the Phusion High-Fidelity DNA polymerase (ThermoFisherScientific). The pET vectors expressing the ASH-C124A, Csl4-F121A and Csl4-F129A variants were generated by site-directed mutagenesis of their wild-type counterparts with appropriate sets of oligonucleotides using the QuikChange II XL Kit (Stratagene) as recommended.

Thermococcus barophilus strains

The chromosomal copy of the TERMP_01768 (encoding *Tba*-ASH-Ski2) and the TERMP_00146 (encoding *Tba*-aRNase J) were deleted by the pop-in/pop-out method to generate the *Thermococcus barophilus* ΔASH-Ski2 and ΔaRNase J strains, respectively using published protocol (37,38).

Production and purification of bait proteins

Escherichia coli BL21-CodonPlus (DE3) cells freshly transformed with pET15-aRNase J, pET15-ASH-Ski2, pET21-ASH-Ski2, pET15-Csl4 or pET15-Rrp41 vectors (Supplementary Table S1) were grown in 400 ml of LB medium at 37°C. Protein production was induced in exponential phase

at an OD_{600nm} of 0.6 by the addition of 0.1 mM IPTG (Isopropyl β-D-1-thiogalactopyranoside). After 3 h of induction at 30°C, the cells were collected, suspended in 10 ml of lysis buffer (50 mM NaPhosphate, 300 mM NaCl, 10 mM Imidazole) supplemented with 1 $mg.ml^{-1}$ of lysozyme and a mix of ethylenediaminetetraacetic acid (EDTA)-free protease inhibitor (cOmpleteTM, Roche) and lysed by sonication (4×[5*10 s], 50% cycle, VibraCell Biolock Scientific). When mentioned, the cleared extracts, obtained by centrifuging the crude extracts (20 000 *g* 4°C, 20 min), were treated with a mix of RNase A (20 $\mu g.ml^{-1}$), RNase T1 ($1U.\mu l^{-1}$) and DNase I (20 $\mu g.ml^{-1}$) containing 10 mM of $MgCl_2$ for 30 min at 37°C. After a heating step at 70°C for 20 min, the extracts were furthered clarified by centrifugation (20 000 *g*, 4°C, 20 min). The recombinant proteins were two-step purified from the soluble fractions to near homogeneity using FPLC (Fast Protein Liquid Chromatography, Äkta-purifier10, GE-Healthcare): first, by a nickel-attached HiTrap chelating column (HisTrap 1 ml, GE-Healthcare) with a linear gradient of 100–500 mM imidazole; secondly, by a heparin column (HiTrap Heparin 1 ml, GE-Healthcare) with a linear gradient of 300 mM to 1 M NaCl. The eluted fractions containing His-tagged proteins were pooled and dialyzed overnight against 500 ml of dialysis buffer (20 mM HEPES pH 7.5, 300 mM NaCl, 1 mM DTT (Dithiothréitol), 10% glycerol buffer).

Co-purification by chromatography affinity

Cells expressing His-tagged bait proteins were produced as described above. Cells expressing untagged prey proteins were obtained after transforming *E. coli* BL21-CodonPlus (DE3) cells with pET11-aRNase J, pET11-ASH-Ski2, pET11-Csl4 or pET11-*Pab*-Rrp41 vectors (Supplementary Table S1) and using the same conditions for growth and induction. Two cell pellets from 200 ml of cultures expressing either bait or prey protein were mixed upon lysis (as before). The bait proteins alone or in complex with the prey proteins were purified by nickel affinity chromatography using Ni^{2+}-NTA column matrices (HisTrap 1 ml, GE-Healthcare). The elution was obtained with a linear 100–500 mM imidazole gradient after washing steps at 10 and 50 mM of imidazole. For each couple of bait/prey that were tested, the co-purification assays were at least performed twice either in presence or absence of RNase/DNase treatment (as above). The proteins from recovered fractions were analysed by Western blotting (4–15% Mini PROTEAN® TGX Stain-Free™ Gels & Trans-blot® Turbo™ Nitrocellulose Transfer Pack, BioRad). The bait proteins were probed using a His Tag HRP-conjugated antibody (Ozyme) diluted 5000-fold. The prey proteins were probed using polyclonal antibodies against *Pab*-aRNase J, *Pab*-ASH-Ski2, *Pab*-Csl4, *Pab*-Rrp41, *Pab*-DnaG or *Pab*-aCPSF1 (custom polyclonal antibodies, Eurogentec) diluted 10 000-fold and an anti-rabbit IgG HRP conjugate (Promega) diluted 5000-fold.

Pull-down by affinity purification assays

The pull-down assays were performed in triplicate with clarified whole-cells extract of *P. abyssi* cultivated on exponential growth phase in bioreactors under physiological conditions (95°C, pH 6.5, anaerobic). The cell extracts were prepared as described in (39). Briefly, *P. abyssi* pelleted cells were re-suspended in 1/3 w/v of 1× phosphate-buffered saline (PBS) buffer (Euromedex), supplemented with 300 mM of NaCl and a mix of EDTA-free protease inhibitor (cOmpleteTM, Roche). After sonication (VibraCell Biolock Scientific), the crude extracts were clarified by centrifugation (20 000 *g*, 30 min, 4°C). Purified His-tagged proteins were used as baits in clarified whole-cell extract of *P. abyssi*. Briefly, 20 μg of bait proteins were immobilized on 0.6 mg of cobalt-coated magnetic beads (Dynabeads, Invitrogen). The complex baits-beads were further incubated with 2 mg of *P. abyssi* extract under rotation for 2 h at room temperature. The protein complexes formed *in vitro* were separated on a magnet and washed extensively with PBS buffer (3*4 ml and 2*1 ml). A second round of pull-down assays was performed with an additional step to eliminate non-specific interaction via DNA or RNA molecules by incubating the protein complexes with an RNase/DNase mix (10 $\mu g.ml^{-1}$ of RNase A and DNase I) for 30 min at room temperature before applying the magnetic force. A control was also performed under identical conditions using cobalt-coated beads alone instead of the baits-beads complexes. Purified protein complexes were eluted in 25 μl of XT sample buffer (BioRad) containing 2 μl of 20× reducing buffer at 95°C for 10 min and separated by sodium dodecyl sulphate-polyacrylamide gelelectrophoresis (SDS-PAGE) short migration on 12% SDS-PAGE (Criterion XT Precast gels–BioRad). After a short migration, the proteins were extracted by cutting out each protein track into one piece followed by shotgun proteomic analyses. For western blot analyses, protein complexes were separated by SDS-PAGE on 4–20% pre-cast Bis-Tris gel (NuPAGE Life technology).

Proteomic analysis

The mass spectrometry analyses were performed at Paris Sud Ouest PAPPSO proteomics core facility (http://papso.inra.fr). Briefly, after a short run on a SDS-PAGE gel, bands of proteins were excised from the gel. In-gel tryptic digestion was performed 6 h at 37°C with 100 ng of modified trypsine (Promega) dissolved in 50 mM NH4CO3. Peptides were extracted with 0.1% trifluoroacetic acid (TFA) and 50% acetonitrile (ACN). Extracted peptides were dried and suspended in 30 μl of 0.05% HCOOH, and 2% ACN. A total of 4 μl of samples were then loaded on a NanoLC-Ultra system (Eksigent). Eluted peptides were analysed on-line with a QExactive mass spectrometer (Thermo Scientific Electron) using a nanoelectrospray interface. Peptide ions were analysed using Xcalibur 2.1 with data-dependent acquisition steps. Peptides were identified with X!TandemPipeline open source software by spectrum matching approach. The mass spectrometry proteomics data have been deposited to the ProteomeXchange Consortium via the PRIDE partner repository with the dataset identifier PXD015856".

The MS data were processed in order to identify specific interaction signals. Global specific spectra from samples were normalized, as described in (40), between replicate series. We used a cut-off of two normalized spectra as

minimum MS signal for network hit validation. Normalized spectra were then averaged between replicates and referenced versus control to calculate the number of 'Referenced Spectra'. Calculation of the 'Specificity Index' score is the ratio of the averaged normalized spectra in control versus assay. The 'Specificity Index' varies from 0 to 1 (with a maximum threshold of 1) as the specificity decreases. For the AP-MS experiments with aRNase J as bait, nuclease and nuclease-free assays were run in triplicate, whereas for ASH-Ski2 the same analyses were performed in 4 replicates. For aRNase J $n = 6$ for the controls and for ASH-Ski2 $n = 8$ for the controls. For ASH-Ski2, we took only into consideration hit proteins detected independently in both His-Tag orientations. The effect of nuclease has been identified as:

$$\text{Nucl. Effect} = 100 \times \frac{\text{Spectra No Nuclease} - \text{Spectra Nuclease}}{\text{Spectra No Nuclease}}$$

Diagram networks have been created using Cytoscape 3.7.2 software (41).

Multiple sequence alignments and phylogenetic tree constructions

The complete archaeal and bacterial genome entries were retrieved from the EBI (European Bioinformatics Institute). The collection of helicases from super-families SF1 and SF2 were identified by RPS-Blast of Pfam domains DEAD (PF00270) or Helicase_C (PF00271) among a set of completely sequenced non-redundant genomes composed of 114 archaeal genomes and 1105 bacterial genomes. A total of 17 661 helicases were identified and further compared to each other using the BlastP program. Partitioning of the all-vs-all Blast results was achieved using the Markov Cluster Algorithm (42) and resulted in 84 clusters of >5 orthologous archaeal helicases. The archaeal sequences were collected and corresponded to occurrences with COG1202 for ASH-Ski2. We also collected an initial set of proteins using COG profile annotations (COG1096 for Csl4 and COG0689 for Rrp41) from complete archaeal genomes. Hidden Markov model (hmm) profiles were built for each family and used with hmmsearch (HMMER package, (43)) to identify homologues in our archaeal proteome sample. In addition, to identify potential unannotated genes and pseudogenes, we performed tblastn searches.

The archaeal phylogenetic tree was inferred from a concatenated dataset of 81 protein families obtained from COG annotation. If multiple copies occurred in a genome, all paralogues were removed. The sequence alignments for each family were created using the MUSCLE program (44) with the default parameters. We used the trimAl program (45) to remove spurious sequences and poorly aligned positions and to analyse the quality of the alignments according to gap numbers and residue conservation in the columns of the alignments. These parsed alignments were concatenated to produce a single alignment of 17 827 residues. When a species did not have a record for a family, the missing sequence was replaced by gaps in the alignment. The maximum-likelihood tree was computed with PhyML (46) and the optimal combinations of parameters was selected using ProtTest3 program (47). The LG model of sequence evolution was used and the gamma-distributed substitution rate variation was approximated by eight discrete categories with shape parameter and proportion of invariant sites estimated from the data. The statistical branch support was inferred with the parametric bootstrap. The archaeal Ski2-like helicase alignment was built by Mafft incorporating local pairwise refinement (L-INS-i) up to 2000 iteration (maxiterate 2000) (48) and trimmed with trimAL as described above. The archaeal ASH-Ski2 helicase tree was computed with the same approach as that of the species tree except that the gamma-distributed substitution rate variation was approximated by four discrete categories. Both trees (species and Ski2-like helicases) were arbitrarily rooted and were drawn with the online version of iTOL (49).

Sucrose gradient fractionation of cell extracts

Pyrococcus abyssi and *T. barophilus* cells were grown at 92°C and 85°C, respectively, in continuous culture in a 5-l Gazlift bioreactor in MES medium under anaerobic conditions at pH 6.8 (50). Cells were maintained in exponential growth phase between 2 and $4*10^8$ cells per ml. After cell culture harvesting at 8°C, Cells were pelleted by centrifugation (10 000 *g*, 20 min at 4°C) and washed two times with a sterile sea salt solution at 30 $g.l^{-1}$. Dry cell pellets were stored at −80°C. A total of 200 mg of cell pellet was re-suspended in 1/3 w/v of buffer TK buffer (20 mM Tris–HCl, 100 mM KCl, 10 mM $MgCl_2$, 1 mM DTT) containing a cocktail of EDTA-free protease inhibitor (cOmpleteTM, Roche) or TK-EDTA buffer (TK buffer supplemented with 20 mM EDTA). Whole-cell extracts were prepared by sonication (10*10 s, 50% cycle, VibraCell-Bioblock scientific). Lysates were cleared at 21 000 *g* for 30 min. Approximately 10 mg of whole-cell extract protein were layered on a linear 10–30% sucrose gradient prepared in TK or TK-EDTA buffers and centrifuged for 5 h at 35 000 rpm at 4°C in Beckman-Avanti XPN-80 SW41 rotor. It was not possible to determine the positions of 30S and 50S ribosomal subunits by classical A254 scanning with the ISCO UA-6 gradient fraction collector due to the inherent colorimetry of the *P. abyssi* and *T. barophilus* cellular extract. For each gradient, 21 fractions of 500 μl were collected. A total of 250 μl of each fraction were precipitated with of 45 μl of 100% trichloacetic acid (TCA). After 30min at −20°C, samples were centrifuged 30 min at 16 000 *g* at 4°C. The protein pellets were washed with 500 μl of glacial acetone (16 000 *g*, 15 min at 4°C), dried and re-suspended in 20 μl of 20 mM Tris–HCL pH 8. After adding 4 μl of 6× loading buffer (375 mM Tris–HCL pH 6.8, 12% SDS, 30% β-mercaptoethanol, 0.6% Bromophenol Blue, 36% glycerol), samples were heated at 95°C for 10 min before proceeding to SDS-PAGE.

Relative quantification of ribosomal RNAs by Slot Blot

A total of 20μl of each fraction collected from sucrose gradient, equally diluted beforehand to set the fraction with the highest nucleic acid content at a concentration of 2.5 $ng.\mu l^{-1}$, was added to 55 μl of denaturation buffer (2.2 M formaldehyde, 50% deionized formamide, 0.5 mM EDTA, 10 mM MOPS, 4 mM NaCl) and incubated at 65°C for 5 min. Each 75 μl-sample was spotted on a nylon membrane (Amersham Hybond-XL; GE Healthcare) by vacuum filtration (PR648-HoeferTM Slot Blot). After UV-crosslinking, blots were hybridized overnight at 42°C with

5′-end P^{32}-labelled oligonucleotides in Roti-Hybrid-Quick buffer (Roth) and washed three times at 42°C for 15 min with SSC buffer (SSC 20×: 3M NaCl, 300 mM sodium citrate, pH 7) containing 0.1% of SDS (5×, 1× and 0.1×, respectively). Sequences of antisense oligonucleotides used to detect *T. barophilus* 16S and 23S rRNAs are listed in Supplementary Table S2. Radioactive signals were visualized on a phoshorImager (Typhoon Trio-Amersham-Bioscience) and quantified using MultiGauge software (Fujifilm).

RESULTS

The protein–protein interaction network of aRNase J includes key components of RNA metabolism

To explore the protein interaction network of the euryarchaeal aRNase J, we carried out affinity purification coupled to mass spectrometry (AP-MS) analyses in *P. abyssi* cell extracts, as already described (39). Recombinant aRNase J from *P. abyssi,* with C-terminal $(His)_6$-tag (aRNase J-His), was produced, purified and used as baits for AP-MS experiments. In order to discriminate specific protein interaction from column background, we performed mock AP-MS analyses with *P. abyssi* cell extracts in absence of protein bait. In addition, to determine if some interactions are mediated through RNA or DNA, we implemented a nuclease treatment after incubating the cell extract with the bait. The co-purified partners were identified by bottom-up proteomic techniques coupled with mass spectrometry. We used an algorithm that prioritizes the specificity of the interaction to classify partners identified in triplicate AP-MS. The list from the most to the least specific is displayed on Supplementary Table S3. Remarkably, we found that aRNase J is at the centre of a protein interaction network that includes proteins with central functions in physiological processes. The pie chart, shown on Figure 1A (left panel), categorizes these processes. A large majority (64%) of the protein partners of aRNase J-His are annotated as involved in RNA metabolism from transcription (RNA polymerase subunits), RNA modification (C/D guide RNP components) and RNA decay (RNA exosome) to translation (ribosomal proteins and translation initiation factors). Amongst protein partners, 14 were detected with a high-specific score in the aRNase J pull-downs whereas no spectra signal were sensed in the controls for these candidates (values of 0 in Supplementary Table S3). Remarkably, the Rrp41 and Rrp42 catalytic core subunits and the Rrp4 cap subunit of the RNA exosome were retrieved among the foremost of the fourteen highly significant protein partners (Supplementary Table S3). Both subunits of the RNA polymerase (RpoA1/A2) were also detected with highly significant scores. Ribosomal proteins and components of the C/D box guide RNP complex are also part of the aRNase J network (51,52). Remarkably, these exploratory analyses reveal PAB2313, a putative ATP-dependent RNA helicase, as a potential partner of aRNase J-His.

In addition, proteins known to be involved in DNA maintenance processes, like RPA41, were also recovered as significant partners (Supplementary Table S3). RPA41 corresponds to the large subunit of the RPA complex that binds to single-stranded DNA. Interestingly, a physical interaction between RPA41 and the RNA polymerase has been previously demonstrated in *P. abyssi* (39). It was revealed that the RPA complex enhance transcription rate *in vitro*, probably via RPA41 interacting with the non-template strand of the elongating complex. In this light, the presence of RPA subunit in the interaction network of aRNase J could be considered as a further evidence for the involvement of aRNase J in RNA metabolism.

Finally, to spotlight protein complexes of aRNase J network, we built a protein interaction map of aRNase-His based on the spectral index of Supplementary Table S3 (Figure 1B). In light of this network, we propose that the 5′-3′ exonuclease aRNase J cross-talks with RNA machineries of the cell.

The *P. abyssi* ASH-Ski2 helicase shares a common network with *P. abyssi* aRNase J RNase and the RNA exosome

Interestingly, in the network of aRNase J, we retrieved PAB2313, a putative RNA helicase, that appears to be a member of the Ski2-like helicase family (53) renowned for their crucial role in RNA decay in eukaryotic cells (54) and we named it ASH-Ski2. To gain further experimental evidence of a coordinated action of aRNase J and ASH-Ski2, we performed new rounds of AP-MS analyses in duplicate with recombinant C- and N-terminal $(His)_6$-tagged versions of *P. abyssi* ASH-Ski2 as baits, respectively, and obtained an exhaustive list of partners (Supplementary Table S4). The ASH-Ski2 partner pie chart shows that a large majority (73%) of identified proteins are annotated as players of RNA metabolism and translation. Indeed, out of 34 in total, 12 ribosomal proteins and four subunits of the RNA exosome are identified as specific partners (Figure 1A, right panel and Supplementary Table S4). Notably, aRNase J is ranked as the first candidate of the ASH-Ski2 partner list of Supplementary Table S4. aRNase J is detected, both with a high-specific score and reference spectra in assays treated or not with nucleases. Furthermore, 21 protein partners are common to both aRNase J and ASH-Ski2 networks (Figure 1B). This highlights a tight cross-talk of aRNase J and ASH-Ski2 in *P. abyssi* cells. It should be noted that several partners of ASH-Ski2 are affected by the nuclease-treatment when compared to aRNase J, which includes the RNA polymerase subunits but also the RNA exosome subunits.

To ensure that aRNase J and ASH-Ski2 are part of the protein interaction network of the RNA exosome, we performed additional pull-down assays, in duplicate, using a purified N-tagged His-Rrp41 of *P. abyssi* as bait. Amongst the pull-downed proteins of the Rrp41 subunit, by western blotting, we specifically detected endogenous Csl4 and DnaG cap subunits, aRNase J and ASH-Ski2, but not the endo-RNase aCPSF1 (Figure 2). Altogether with the limitation that the pull-down was performed with the sole Rrp41 subunit and not with a re-formed complex with the Rrp42 core and Csl4/Rrp4 cap subunits, these results support a potential interplay between aRNase J, ASH-Ski2 and components of the archaeal RNA exosome in *P. abyssi* cells. This is thoroughly consistent with the results of the above AP-MS analysis set.

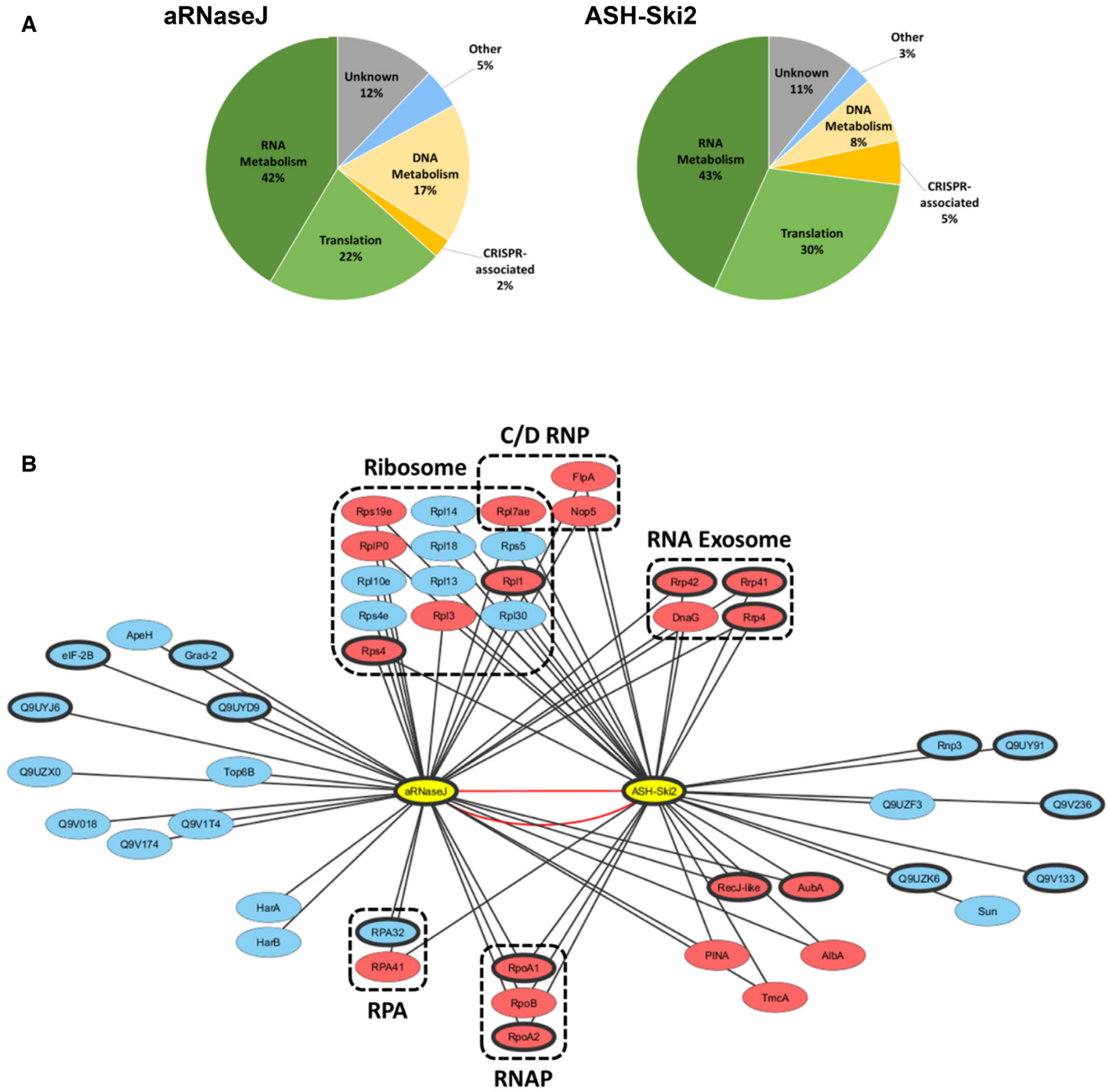

Figure 1. (**A**) Functional classification pie charts of proteins identified by pulldown-MS/MS approach using recombinant aRNase J and ASH-Ski2 as baits, respectively. (**B**) Network of protein partners for aRNase J and ASH-Ski2. The aRNase J and ASH-Ski2 baits are labelled in yellow. Network backbone is represented in black lines except for ASH-Ski2 and aRNase J for which reciprocal interactions are in red. Common partners of ASH-Ski2 and aRNase J are indicated in pink whereas specific partners are indicated in blue. Bolded circle indicate highly specific hits, absence in all control runs, with a 'spectra index' of 0 (see Supplementary Tables S3 and 4).

The archaeal ASH-Ski2 members share identical taxonomic distribution as aRNase J members

To gain insights into the relationship that exists between archaeal aRNase J and ASH-Ski2 members as well as with the RNA exosome subunits, we compared their taxonomic distributions amongst the archaeal phylogeny. To do so, we first upgraded a phylogenomic study of the superfamily of the archaeal SF2 helicase (53) in order to accurately identify the Ski2 family of helicases encoded in archaeal genomes. In contrast to the role of eukaryotic Ski2-like RNA helicases in RNA homeostasis, reports on the functions of archaeal Ski2-like helicase family members are still scarce. As a common theme throughout SF2 helicase families, the unique characteristics of Ski2-like family members are mainly derived from accessory domains that decorate the helicase core and provide additional functionalities (55,56). Ski2-like helicase structures demonstrate that the molecular 'core' of all Ski2-like helicases is a ring-like

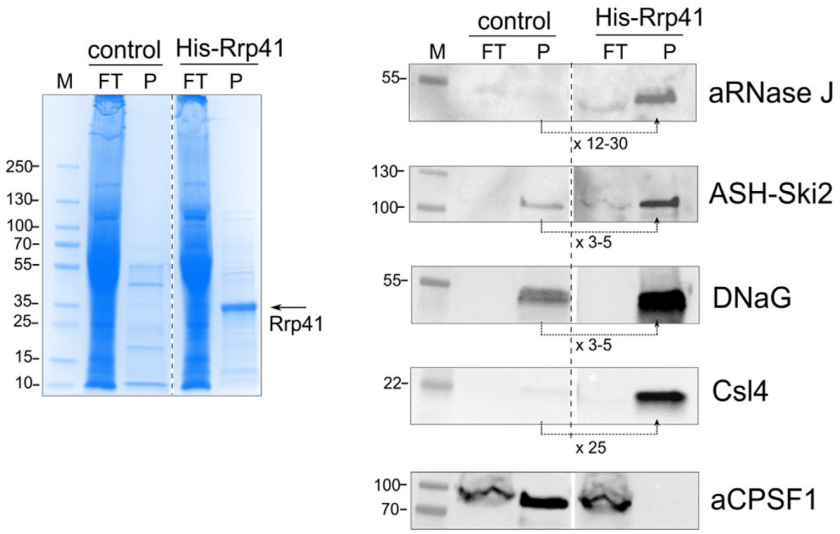

Figure 2. Pull down assays using the recombinant (His)-Rrp41 protein as bait in whole-cell extracts of *Pyrococcus abyssi*; FT corresponds to the flow through, P to the pull-downed fraction and M to the protein ladder. Each fraction was analysed by Coomassie blue staining of SDS-PAGE (left panel) and by western blotting using specific antibodies for aRNase J, ASH-Ski2, DnaG, Csl4 and aCPSF1 (right panel). To highlight the pull-downed proteins, the relative signals were average from two independent assays as indicated below each panel.

four domain assembly of two RecA domains, a winged helix domain and a ratchet domain (54,57). By performing RPS Blast searches, we retrieved all archaeal Ski2-like helicase member sequences from 147 non-redundant completely sequenced archaeal genomes. In addition to Hel308 members, characterized by the COG 1204 and documented with enzymatic features of DNA helicases (54,58–61), we also retrieved the ASH-Ski2 group, characterized by the COG 1202 (53). Interestingly ASH-Ski2 members hold an additional N-terminal domain in which four strictly conserved cysteines have the propensity to form a zinc-finger-like motif (62) (Figure 3A). ASH-Ski2 members are specific of euryarchaeal phylogenetic groups with the Lokiarchaeum as an exception (Figure 3B). Remarkably aRNase J and ASH-Ski2 members present similar occurrence, which is restricted to most euryarchaeal groups, with the exception of the archeoglobales and thermoplasmatales. Furthermore, the co-evolution of aRNase J and ASH-Ski2 members shown by the comprehensive congruence of aRNase J and ASH-Ski2 phylogenetic trees, with only few observed leaf displacements within taxonomic groups, reinforces their potential functional interplay (Supplementary Figure S1). Altogether, protein networks combined with our phylogenomics analyses argue for a coordinated action of aRNase J and ASH-Ski2 in specific cellular processes in Euryarchaeota.

Subsequently, we compared the taxonomic distribution of aRNase J, ASH-Ski2 and the RNA exosome Rrp41 and Csl4 subunits along the archaeal phylogeny (Figure 3B). Like in our previous studies (15,27), we showed that the RNA exosome is not present throughout the whole archaeal taxonomy and that aRNase J, as well as ASH-Ski2, do not follow the taxonomic distribution of RNA exosome components. Indeed, it is absent from the Halobacteria and Methanomicrobiales members for which the 3′-5′ exoribonucleolytic activity is carried by another enzyme, the aRNase R (14,15). In the Methanococci group, no enzyme with equivalent activity could be, so far, detected by comparative genomics.

aRNase J forms a stable complex with the helicase-like ASH-Ski2, *in vitro*

To investigate a direct interaction between aRNase J and ASH-Ski2, we used an *in vitro* co-purification assay on nickel affinity chromatography to test pairwise interactions. A recombinant $(His)_6$-tagged bait (His-ASH-Ski2) and an untagged prey (aRNase J) from *P. abyssi* were expressed independently in *E. coli* cells using the pET15b and pET11b expression vectors, respectively (Supplementary Table S1). Cells over-expressing the recombinant $(His)_6$-tagged bait or the untagged prey proteins were mixed in a 1:1 ratio prior the lysis step. After nucleic acids removal with a cocktail of nucleases, most of the proteins from *E. coli* were eliminated at 70°C for a specific enrichment of the thermo-resistant proteins from *P. abyssi*. The clarified cellular extracts were then injected on a nickel column to retain the bait His-ASH-Ski2 protein and its potential interacting partners. Washing steps with low imidazole concentrations served at removing weakly bound contaminants. The bait and the retained interacting proteins were eluted with a linear gradient of imidazole. The protein content of each recovered fractions was analysed by SDS-PAGE. The specific presence of aRNase J and His-ASH-Ski2 was revealed by western blotting using specific antibodies as shown in Figure 4A. As expected, aRNase J co-elutes with His-ASH-Ski2 even after nucleic acids removal. This establishes that, at high temperature and ionic strength (300 mM NaCl), aRNase J and His-ASH-Ski2 associate to form a stable complex that is not mediated through RNA or DNA molecules (Figure 4A, top panel). As a control, to demonstrate that protein co-purification is a consequence of complex formation rather than non-specific interactions with the column matrices, we controlled that untagged versions of aRNase J or ASH-Ski2

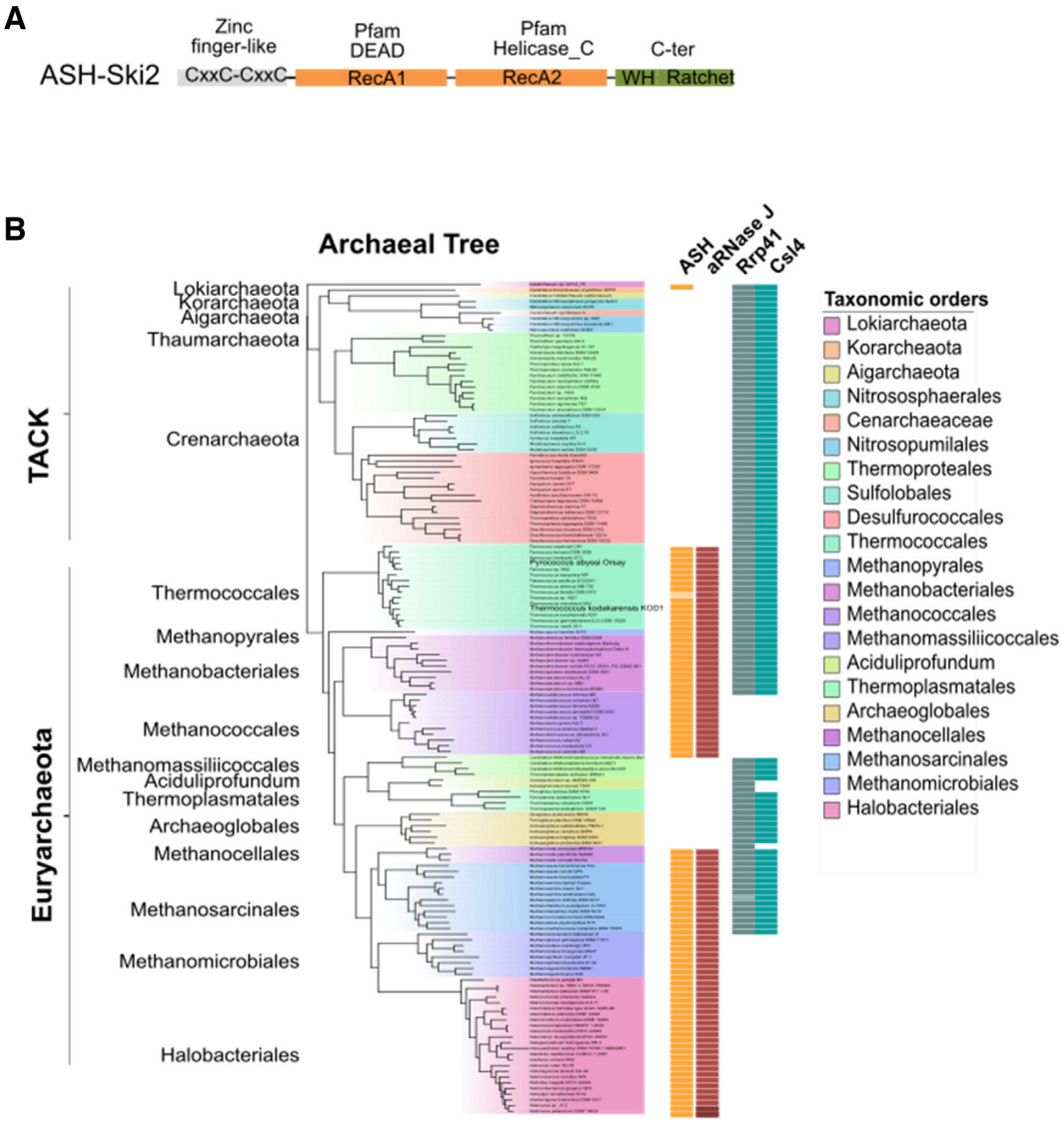

Figure 3. (**A**) Schematic protein domain architecture of the ASH-Ski2 group. The common SF2 core is composed of the RecA1 and RecA2 subdomains (Pfam DEAD & Helicase_C) in orange, of the C-terminal domain in green and of the N-terminal domain in grey. The strictly conserved cysteine residues of the N-terminal domain are represented. **(B)** Taxonomic distributions of ASH-Ski2, aRNase J and Rrp41/Csl4 from the RNA exosome among archaeal genomes. Their occurrence is plotted and juxtaposed to the archaeal specie tree. Taxonomic orders and Pfam domains are colour coded. Darker and lighter shades indicate multiple copies and pseudogenes, respectively.

are not intrinsically retained on Ni^{2+}-NTA column matrices (Supplementary Figure S2A). Despite the robustness of these data, we cannot completely exclude a stabilization of an ASH-Ski2 /aRNase J complex by remaining *E. coli* proteins like ribosomal proteins that are highly abundant. However, we have additional evidence supporting an interaction between aRNase J and ASH-Ski2. By comparing the sedimentation profiles (5–25% sucrose gradient) of each individual purified protein to the one obtained with a mixture of both (Supplementary Figure S2B), we showed that the sedimentation profile of aRNase J is affected by the presence of ASH-Ski2. Indeed, whilst the sedimentation profile of aRNase J alone most likely corresponds to its homotetrameric form as observed for *Methanolobus psychrophilus* aRNase J in solution (63), in presence of ASH-Ski2, a significant proportion of aRNase J is shifted to fractions of different molecular weight. This shift is most likely due to an interaction with ASH-Ski2 that is found in the same fractions as aRNase J.

To uncover which protein domain of ASH-Ski2 is specifically involved in the formation of a complex with aRNase J, variants of His-ASH-Ski2 were used as baits for the untagged prey aRNase J. Pairwise interactions were tested as previously described performing *in vitro* co-purification assays (Figure 4A, lower panels). Our results indicate that the accessory C-terminal domain of ASH-Ski2 (His-ΔC) is not required in establishing an *in vitro* interaction with aRNase J as the elution profile is comparable to the one with full-length ASH-Ski2. In contrast, the accessory N-terminal domain of ASH-Ski2 (His-ΔN) seems to be critical for the in-

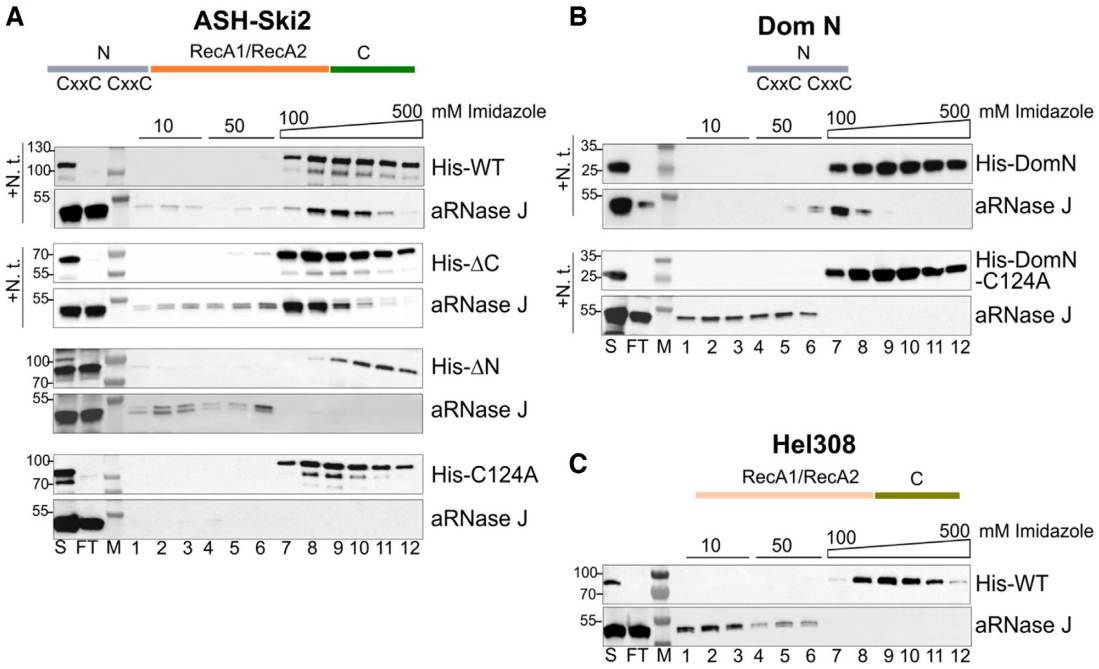

Figure 4. *In vitro* co-purification assay of aRNase J challenged by His-ASH-Ski2 and His-Hel308. (**A**) Schematic representation of the protein domain architecture of ASH-Ski2 from *Pyrococcus abyssi* and affinity co-purification assays on nickel chromatography column of recombinant untagged aRNase J with His-ASH-Ski2 and its variants. The full-length protein (His-WT), deleted for the C-terminal (His-ΔC) and N-terminal (His-ΔN) domains or harbouring a punctual substitution of the conserved cysteine residue into alanine (His-C124A) were used as baits. The fractions were analysed by western blotting using an His-Tag or a specific antibody against aRNase J. S: supernatant loaded on the affinity Nickel column; FT: flow through; 10 mM (lanes 1–3) and 50 mM (lanes 4–6) imidazole washing steps; Elution with an Imidazole gradient from 100 to 500 mM (lanes 7–12). Experiments performed with nuclease treatment (+Nt) are indicated on the left of each panel. (**B**) Assays as performed in (A) with the wild-type N-terminal domain DomN (His-WT) or containing the C124A substitution (His-C124A) of ASH-Ski2. (**C**) Assays as carried in (A) but with His-Hel308 as the protein bait.

teraction since aRNase J does not co-elute with the ΔN variant of ASH-Ski2. Finally, we showed that the accessory N-terminal domain of ASH-Ski2 expressed alone (His-DomN) is sufficient to establish an *in vitro* interaction with aRNase J (Figure 4B, top panel).

The sequence alignment of the N-terminal domains of archaeal ASH-Ski2 highlights the presence of four strictly conserved cysteines with the propensity to form a zinc finger-like motif (Figure 4A). To test whether this motif is critical for the interaction between ASH-Ski2 and aRNase J, we substituted the C124 residue of full-length His-ASH-Ski2 and His-DomN by an alanine (A) and we challenged their capacity to retain aRNase J on Ni^{2+}-NTA column as before. Our results show that the conserved C124 residue is critical in establishing or in stabilizing an interaction between the full-length or DomN of ASH-Ski2 and aRNase J (Figure 4A and B, lower panels). Indeed, the single C124A substitution is sufficient in destabilizing this interaction.

Finally, to confirm the specificity of the interaction between aRNase J and ASH-Ski2, we performed similar *in vitro* co-purification assays using aRNase J as a prey and His-Hel308, another Ski2-like helicase encoded in the *P. abyssi* genome, as bait. In this configuration, aRNase J is not retained on the Ni^{2+}-NTA column matrices (Figure 4C) meaning that aRNase J specifically interacts with ASH-Ski2. This result is not surprising as members of the Hel308 family do not possess the N-terminal zinc finger-like motif extension.

aRNase J forms a complex with the exosome cap-subunit Csl4 *in vitro*

We also tested the pairwise interactions between aRNase J or ASH-Ski2 and RNA exosome subunits that are among the most retrieved proteins with aRNase J and ASH-Ski2 in the AP-MS analyses (Figure 1B; Supplementary Tables S3 and 4). The results of the *in vitro* co-purification assays performed as described above are summarized in Figure 5A. First, we challenged the catalytic subunit His-Rrp41 as bait with aRNase J or ASH-Ski2 as preys. Only aRNase J could be recovered in the elution fractions together with His-Rrp41. The Rrp41/aRNase J complex is nucleic acid-dependent since its formation is sensitive to nuclease treatment (Figure 5B). Then, we challenged the exosome cap subunits His-Rrp4, DnaG-His or His-Csl4 as baits with aRNase J or ASH-Ski2 as preys. In our conditions, neither Rrp4 nor DnaG were found to interact with aRNase J (Supplementary Figure S2C) or Rrp4, DnaG nor Csl4 with ASH-Ski2 (Supplementary Figure S2D). In contrast, the exosome cap-subunit Csl4 is able to form a complex with aRNase J that is not sensitive to nuclease treatment and therefore is not mediated by nucleic acids (Figure 5C). To go further in the characterization of this association, we then searched for the protein domains of Csl4 that are involved in the formation of the Csl4/aRNase J complex. Whilst the N-terminal domain of Csl4 (ΔN) is not required, its C-terminal domain (ΔC) is critical for the formation of the Csl4/aRNase J complex (Figure 5C).

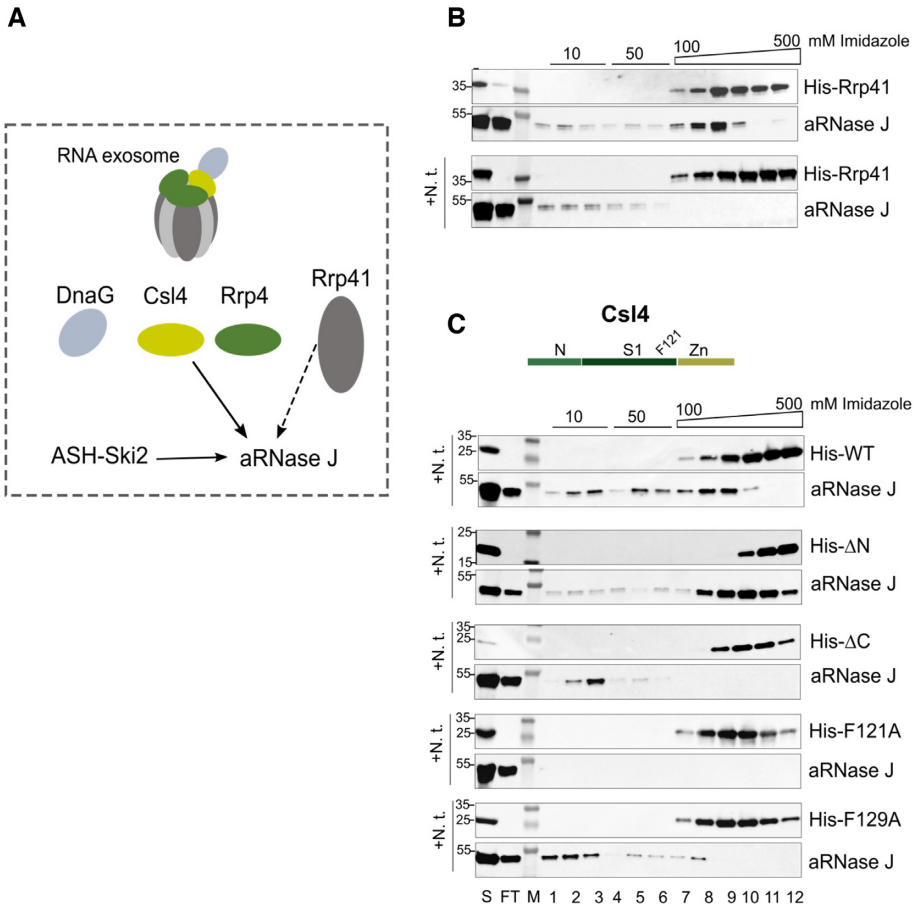

Figure 5. *In vitro* interaction of ASH-Ski2 and aRNase J with the RNA exosome subunits. (**A**) Schematic representation of the RNA exosome machine and of the pairwise interactions detected in this study. Plain arrows indicate interactions resistant to nuclease treatment. Dotted arrows indicate interactions sensitive to nuclease treatment. The *in vitro* co-purification assays of ASH-Ski2 or aRNase J challenged by His-Csl4 are shown in (**B**) and (**C**), respectively. The schematic representation of the protein domain architecture of Csl4 is shown (see also Supplementary Figure S3B). Wild-type Csl4 (His-WT) and variants with a deletion of the C-terminal (His-ΔC) or N-terminal (His-ΔN) or a punctual substitution of phenylalanine 121 in alanine in the S1 domain (His-F121A) were used as baits. Legend details are as in Figure 4.

To highlight specifically conserved residues in Csl4 sequences that are co-distributed with aRNase J, we derived weblogos from multiple alignments of Csl4 co-distributed or not with aRNase J. Several positions (including F/Y121 and F129, numbering according to the *P. abyssi* sequence) in the S1 domain of Csl4 could be identified as highly conserved in Csl4 sequences in the context of the co-distribution with aRNase J (Supplementary Figure S3A). Strikingly, the phenylalanine residues, F121 and F129, located on the central S1 domain of Csl4 and solvent-exposed in the *P. abyssi* Csl4 structural model (Supplementary Figure S3B) are also key for the association with aRNase J (Figure 5C).

aRNase J and ASH-Ski2 and the RNA exosome co-sediment with high molecular weight complexes in sucrose gradient fractionation of whole-cell extract from *P. abyssi and Thermococcus barophilus*

Altogether, our results propose a tight relationship between aRNase J, ASH-Ski2 and the RNA exosome. Here, we asked whether these protein partners could form higher order protein complexes in archaeal cells. To this end, we discriminated the sedimentation profile behaviours of endogenous aRNase J, ASH-Ski2 and Rrp41 in two Thermococcales organisms, *T. barophilus* (*Tba*) and *P. abyssi* (*Pab*) by doing ultracentrifugation of whole-cell extracts on continuous 10–30% sucrose density gradient (Figure 6A and Supplementary Figure S4A, respectively). Since to this date, *P. abyssi* cannot be genetically modified, the *T. barophilus* strain was used as a genetically tractable model (37,38) to assess the sedimentation profile of endogenous aRNase J in absence of ASH-Ski2 and vice-versa. Moreover, note that the antibodies produced to detect our proteins of interest from *P. abyssi* by immunoblotting cross-react with their counterparts from *T. barophilus* whilst preserving their specificity. Unexpectedly, the vast majority of these proteins co-sediment in heavy fractions with barely any signal in light fractions. This is not the case for the β-CASP endoRNase *Pab*-aCPSF1, which was not identified in any of the protein interaction networks that we uncovered in this study (Supplementary Figure S4). It is interesting to note that *Pab*/*Tba*-aRNase J and *Pab*/*Tba*-ASH-Ski2 are similarly distributed through the gradient (Figure 6A and Supple-

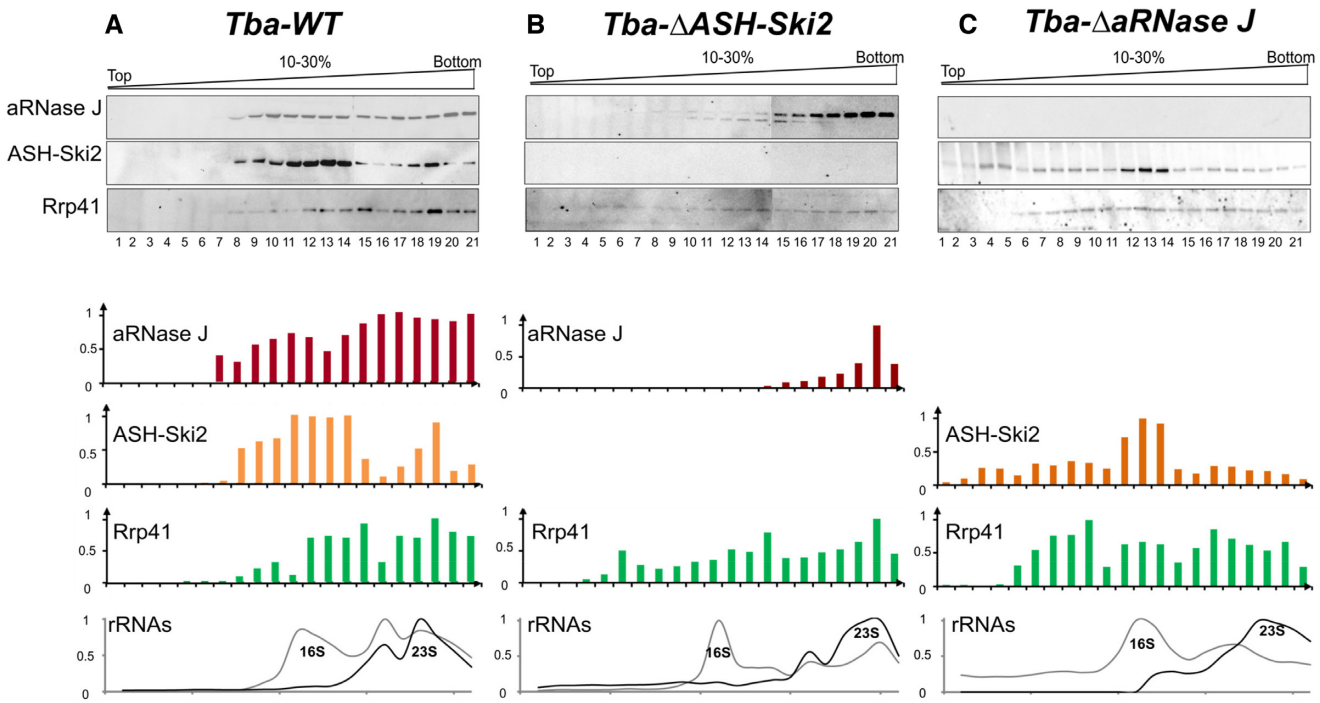

Figure 6. Sedimentation profiles of endogenous aRNase J, ASH-Ski2 and Rrp41 of *Thermococcus barophilus* wild-type (WT) in (**A**), ΔASH-Ski2 in (**B**) and ΔaRNase J in (**C**), strains. Clarified whole-cell extracts were fractionated on 10–30% density sucrose gradients by ultracentrifugation. Equal volumes of fraction, precipitated with TCA, were monitored by western blotting using specific antibodies. The digital images and bar charts representing the relative amounts of protein are given. The ribosomal RNAs were also profiled by slot blotting equal volume of denatured fractions with probes complementary to 16S and 23S rRNAs. The relative quantification of 16S and 23S ribosomal RNAs is plotted in grey and black, respectively.

mentary Figure S4). This distribution pattern is also highly similar to the one of the RNA exosome subunit *Pab*/*Tba*-Rrp41 (Figure 6A and Supplementary Figure S4). In conclusion, our data are indicative of a co-migration of the *Pab*/*Tba*-aRNase J, the *Pab*/*Tba*-ASH-Ski2 and the Rrp41 RNA exosome subunit in high molecular weight fractions.

To go further, we fractionated whole-cell extracts from *T. barophilus* strains enclosing a deletion of the gene encoding *Tba*-ASH-Ski2 (*Tba-ΔASH-Ski2,* Figure 6B) or *Tba*-aRNase J (*Tba-ΔaRNase J*, Figure 6C). On one hand, when *Tba*-ASH-Ski2 is missing, most of the endogenous *Tba*-aRNase J protein is shifted towards the bottom of the gradient. On the other hand, when *Tba*-aRNase J is not present, the distribution profile of the endogenous *Tba*-ASH-Ski2 is also clearly altered; but in this case, *Tba*-ASH-Ski2 is more evenly spread out along the gradient. Note that the profile of the core RNA exosome subunit, Rrp41, was barely affected in both genomics contexts. Overall, these results strongly suggest that the aRNase J & ASH-Ski2 are part of higher-order complexes in *T. barophilus* cells. In addition, we observe that the 16S and 23S ribosomal RNA profiles overlap the ones of aRNase J, ASH-Ski2 and Rrp41. In absence of ASH-Ski2, aRNase J is shifted towards the ribosome. From these results and in light of data reported for bacterial RNase J and eukaryal Ski2 helicases (64,65), we propose that these two enzymes cooperate with the ribosome in Thermococcale cells.

We also challenged the physical association of *Tba*-aRNase J and *Tba*-ASH-Ski2 in higher-order complexes, by performing similar fractionation assays but at low magnesium concentration (TK-EDTA buffer) (Supplementary Figure S5). In these conditions, the assembled ribosomes dissociate into individual subunits (66). In the wild-type strain, endogenous *Tba*-aRNase J and *Tba*-ASH-Ski2 co-sediment with the 16S and 23S rRNAs from the small and large subunits, respectively (Supplementary Figure S5A). Again, we observe a perfect overlay of the sedimentation profiles of *Tba*-aRNase J and *Tba*-ASH-Ski2 as previously seen at a higher concentration of magnesium (Figure 6A and Supplementary Figure S5A). Similar results were obtained with extracts from *P. abyssi* cells (Supplementary Figure S4B). More interestingly, in absence of crosstalk with ASH-Ski2, a flagrant alteration of the sedimentation behaviour of *Tba*-aRNase J was also detected. Indeed, in the context of the *Tba-ΔASH-Ski2* strain, at low magnesium concentration, *Tba*-aRNase J is shifted from the bottom of the gradient to fractions overlapping the profiles of the 16S and 23S rRNAs (Supplementary Figure S5B). In absence of *Tba*-aRNase J, we observe overlay sedimentation profiles of *Tba*-ASH-Ski2 and *Tba*-Rrp41 (Supplementary Figure S5C). From these results, we argue for an association of aRNase J with ribosome/polysome that is emphasised in absence of ASH-Ski2 in addition to an interplay between aRNase J, ASH-Ski2 and Rrp41 RNA exosome subunit.

DISCUSSION

Elucidating the RNA processing machineries is of a critical importance to understand the molecular basis of RNA decay and processing in Euryarchaeota. In this study, to

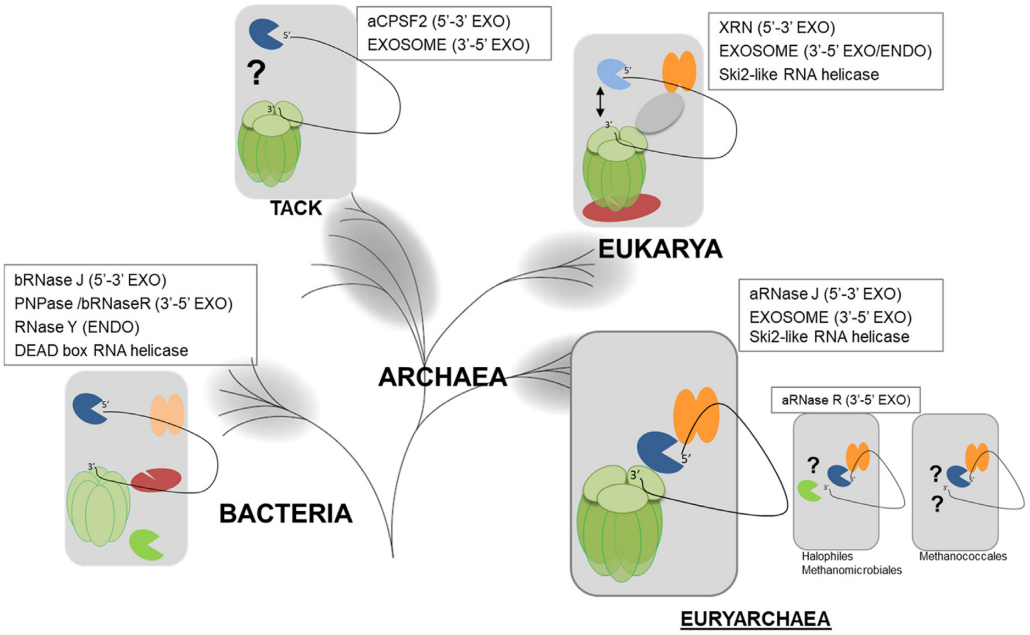

Figure 7. Schematic representation of the interplay between enzymes and machineries in charge of 5′-3′ and 3′-5′ RNA decay and surveillance in the three domains of life. The life tree model is as in (84). The 3′ end RNA trimming activity is carried by the RNA exosome machinery (barrel in green and cap in light green) in most Archaea (15) and Eukarya (76) that is similar to bacterial PNPase (barrel in light green). In Halobacteria and Methanomicrobiales the aRNase R, orthologous to bRNase R, (green packman) carries the 3′-5′ exo activity. In Methanoccocci, no 3′-5′ exo activity has yet been described (15). The 5′-3′ exoribonucleolytic activities (blue packman) are carried by XRN RNases in Eurkarya (85), bRNase J and aRNase J in Bacteria and Euryarchaea and aCPSF2 in the TACK group. RNA helicase activities shown to be involved in RNA surveillance belong to the Ski2-like family in Eukarya (42) and Euryarchaea (this study) and to the DEAD box family in Bacteria (86). The interplay between 5′-3′ and 3′-5′ exoribonucleolytic activities are reported to take place in the RNA-degradosome-like complex in Bacteria that also involves endoRNases (red packman) (87) and through the 5′-3′ communication by a 'closed-loop' architecture of mRNA in Eukarya (88). In most Euryarchaea, we propose that aRNase J/ASH-Ski2 complex interplays with the RNA exosome. In the TACK group and the Halophiles, Methanomicrobiales and Methanoccocales, such an interplay remains to be characterized (question marks).

our knowledge, we provide the first experimental evidences hinting at the existence of high-order β-CASP protein complex(es) in Thermococcales that would carry 5′-3′ & 3′-5′ exoribonucleolytic and helicase-like activities and that could play pivotal roles in archaeal RNA surveillance. First, we identified the interaction landscape of aRNase J from *P. abyssi*, a 5′ to 3′ β-CASP exoRNase (32). Candidate partners include, notably, a Ski2-like helicase ASH-Ski2, the archaeal RNA exosome that exhibits 3′ to 5′ exoribonucleolytic and 3′ end-tailing activities (17) and ribosomal proteins. Of high significance, we also found these proteins to be candidate partners in the interaction landscape of ASH-Ski2 and in the pull-down of the core exosome subunit Rrp41 (Figures 1B and 2). In addition, we showed that aRNase J is able to interact, *in vitro,* with ASH-Ski2 and the exosome cap subunit Csl4 (Figures 4 and 5). Our *in vitro* data are strengthened by our phylogenomic studies showing that, with only one exception, ASH-Ski2 is only encoded in archaeal genomes that carry a gene for aRNase J and that amino acids of Csl4, involved in the *in vitro* interaction with aRNase J, are only conserved in archaeal genomes where their encoding genes are co-distributed (Figure 3). Finally, our *T. barophilus* whole-cell extract fractionation experiments provide evidences that an aRNase J/ASH-Ski2 complex might exist *in vivo* as their sequential deletions modify the sedimentation profile of their protein partner (Figure 6). Individually, aRNase J and ASH-Ski2 do not appear to be essential in *T. barophilus* in optimal growth conditions. However, we could not obtain a strain that combined both gene deletions. This synthetic lethality as demonstrated in yeast for genes involved in same RNA degradation pathways (67,68) strongly hints at a functional relationship between aRNase J and ASH-Ski2 in Thermococcales.

In conjunction with our previous demonstration that β-CASP RNases, ubiquitous in Archaea, must be key players in archaeal RNA metabolism (26,27), our current data support a model whereby the β-CASP RNase, aRNase J, the ASH-Ski2-like helicase and the RNA exosome interplay in most euryarchaeal cells (Figure 7). It remains to determine how this interplay could impact the archaeal RNA metabolism. Since our data imply that ASH-Ski2 has an impact on aRNase J and *vice versa*, we favour a scenario where, at least, ASH-Ski2 and aRNase J have a functional connection. This is all the more so given that aRNase J and ASH-Ski2 show a taxonomic co-distribution amongst the archaeal phylogeny and nearly perfect phylogenetic tree congruence suggesting a co-evolution and potentially an ancient origin (Figure 3B and Supplementary Figure S1, respectively). Based on what is known about the role of these factors in Eukarya and Bacteria, we discuss what we believe to be the most probable scenarios. Evidently, further work will be needed to determine how these proteins alone or in complex shape the euryarchaeal RNA metabolism.

First, recent published work proposes that ASH-Ski2, also named Eta for euryarchaeal termination activity, influences transcription termination by disrupting archaeal transcription elongation complex (69). However, as its helicase activity is rather slow and cannot keep up with wild-type RNAP elongation rates, Eta was recently proposed to be more likely involved in the rescue of transcriptional arrest (70). In our study, the presence of RPA and RpoB subunits in the interaction network of ASH-Ski2 could be a further evidence for the involvement of ASH-Ski2 in the transcription. In addition, transcriptional termination and rescue pathways also involve proteins with ribonucleolytic activities. In Eukarya, the 5′-3′ exoribonucleolytic activity of Rat1p/Xrn2p was proposed to be associated in a transcription termination pathway called 'torpedo model' (71). In chloroplast, RNase J was shown to play a critical role in removing antisense RNAs that are generated by read-through transcription (72). Nevertheless, chloroplast RNase J exhibits a DNA binding domain found in transcription factors of plants that is not present in archaeal RNase J and that could be essential to fulfil this function (73). Finally, co-factors of the nuclear RNA exosome were shown to connect transcription termination to RNA processing by guiding terminated transcripts to the appropriate exonuclease (74). In Archaea, it is still not known if a ribonucleolytic activity is critical since, until now, the complete picture of transcription termination is far from being understood (70). It remains to identify if aRNase J, ASH-Ski2 and the RNA exosome are involved together or alone in transcription termination or rescue pathways which have been shown to be key in influencing the fate of a transcribed RNA.

Moreover, based on the roles of the Ski2-like helicases in Eukarya (75), the idea that the euryarchaeal ASH-Ski2 group is closely connected to RNA-related pathways emerges (Figure 7). Indeed, eukaryal Ski2, Mtr4 and Brr2 which are described as RNA helicases that process RNAs in a 3′-5′ direction were shown to play critical roles in RNA decay, surveillance and splicing, respectively (54,75). Notably, Ski2 and Mtr4 are essential co-factors of the cytoplasmic and nuclear RNA exosomes, respectively, by being involved in the recruitment of RNA substrates (13). Likewise, our work provides several evidences of interplay between the archaeal RNA exosome and ASH-Ski2. Our data also suggest that this interplay is done through aRNase J that interacts *in vitro* with Csl4 from the RNA exosome cap and with ASH-Ski2. Altogether, our results converge towards a cross-talk between the 5′-3′ and 3′-5′ exo-ribonucleolytic activities carried by aRNase J and the RNA exosome, respectively. This is consistent with what is observed in Eukarya, where mounting evidences show a functional interplay between surveillance pathways taking place at the 5′ and 3′-ends of RNAs (76) (Figure 7).

Finally, it must be remembered that aRNase J is the homologue of bacterial RNase J (bRNase J) which was shown to be critical in mRNA decay and rRNA maturation pathways and to be part of a degradosome-like complex (29,77–78). bRNase J which can carry 5′-3′ exo- and endo-RNase activities was shown to associate with proteins identified as, among others, helicase-like proteins and a polynucleotide phosphorylase (PNPase). Bacterial PNPase form an RNA-degradation machine with 3′-5′ exoribonucleolytic and polyadenylation activities reminiscent to the archaeal RNA exosome (79) (Figure 7). Although, in some organisms, the bRNase J degradosome-like complex appears to be transient and dynamic, limiting its validation *in vitro*, this is consistent with interplay between 5′-3′ and 3′-5′ RNA surveillance decay in Bacteria. Therefore, it emerges that, in the three domains of life, RNA surveillance could be taken care of by evolutionary conserved RNase-based RNA-degradation machines with RNA helicase and with 5′-3′ and 3′-5′ exoribonucleolytic activities (Figure 7).

From cellular fractionation assays, we observed that both aRNase J and ASH-Ski2 could potentially associate with the ribosome. Interestingly, it was also shown that bRNase J can associate with translating ribosomes (64) and the crystal structure of the eukaryotic 80S ribosome-Xrn1 complex showed that the 5′-3′ Xrn1 nuclease binds at the mRNA exit site of the ribosome (80). Since the sedimentation profiles of *T. barophilus* and *P. abyssi* aRNase J resemble to the one reported for the eukaryal 5′-3′ exo-RNase Xrn1, we speculate that the archaeal aRNase J is also associated with polysomes in Thermococcales cells. This is reminiscent of what is described in eukaryal mRNA surveillance pathways (28) in which mRNA decay is initiated by an endonucleolytic cleavage of ribosome-associated mRNAs (81,82), followed by rapid degradation in the 3′-5′ direction by the RNA exosome or in the 5′-3′ direction by Xrn1 (83). Recently, direct experimental evidence showed that the cytoplasmic RNA exosome is able to interact with the ribosome through a direct interaction mediated by the SKI complex (composed of Ski2-Ski3-Ski8 factors). More precisely, it was shown that ribosome binding displaces the autoinhibitory domain of the Ski2 RNA helicase (65).

On a side note, it is important to notice that the RNA exosome is not present throughout the whole archaeal taxonomy (15,27) and that aRNase J does not accurately follow the taxonomic distribution of RNA exosome components. In the Halophiles that do not encode the exosome subunits, the 3′-5′ exo-ribonucleolytic activity is carried by another enzyme, the aRNase R (14,15). It would be interesting to know whether the halophilic and methanomicrobiale aRNase J, alone or in complex with ASH–Ski2 complex, interplays with aRNase R. In the Methanococci group, no 3′-5′ exo-RNase could be detected by comparative genomics. In this case, aRNase J might connect to specific archaeal RNases that remain to be identified (Figure 7). In conclusion, this work establishes a solid base in the largely overlooked but extremely important field of archaeal RNA metabolism. We identified two phylogenetical conserved factors in Euryarchaea, the 5′-3′ exo-RNase aRNase J and the Ski2-like helicase ASH-Ski2, which have homologues in Bacteria and Eukarya, respectively (Figure 7). Therefore, a mosaic system in Euryarchaeota could be at the centre of networks interplaying with the archaeal RNA exosome and the ribosome. This is an example showing that Archaea use composite systems and thereby elucidating mechanism in archaeal organisms could give valuable insights into understanding function and evolutionary routes of protein networks or/and high-order complexes. Analogous to eukaryal and bacterial systems, we propose that these factors act in partnership in major archaeal RNA decay or surveillance pathways. Deeper insights need to be

gained into the function and importance of these enzymes in mRNA decay, ribosomal RNA maturation, mRNA 3′-end formation and transcription termination. It remains, among other aspects, to be established how these factors might be involved in shaping the RNA landscape in euryarchaeal cells. Finally, the settlement of specific enzymatic properties of ASH-Ski2 and the determination of structure-function of ASH-Ski2/aRNase J and Csl4/aRNase J complexes will ascertain their physiological functions in the context of the interplay with aRNase J.

DATA AVAILABILITY

The mass spectrometry proteomics data have been deposited to the ProteomeXchange Consortium via the PRIDE partner repository with the dataset identifier PXD015856.

SUPPLEMENTARY DATA

Supplementary Data are available at NAR Online.

ACKNOWLEDGEMENTS

We are indebted to L. Correia of the Paris Sud Ouest PAPPSO proteomics core facility (http://papso.inra.fr) which is supported by INRA (http://www.inra.fr), the Ile-de-France regional council (https://www.iledefrance.fr/education-recherche), IBiSA (https://www.ibisa.net) and CNRS (http://www.cnrs.fr) for LC/MS analyses and to L. Correia. We thank Y. Quentin for its expertise in taxonomic identification of archaeal Csl4 and Rrp41 members, L.Plassart and J. Caumes for technical help and P. Vitali and M. Kwapisz for helpful discussions.

FUNDING

CNRS; University Paul Sabatier; University of Western Britany; Ifremer; University of Toulouse, Idex-emergence program (to B.C.O.); French Ministère de l'Enseignement Supérieure et de la Recherche PhD Fellowship (to D.K.P and C.E.); French 'Agence Nationale pour la Recherche' [ANR-16-CE12–0016 to B.C.O]; Funding for open access charge: ANR [ANR-16-CE12-0016-01].
Conflict of interest statement. None declared.

REFERENCES

1. Moissl-Eichinger,C., Pausan,M., Taffner,J., Berg,G., Bang,C. and Schmitz,R.A. (2018) Archaea are interactive components of complex microbiomes. *Trends Microbiol.*, **26**, 70–85.
2. Adam,P.S., Borrel,G., Brochier-Armanet,C. and Gribaldo,S. (2017) The growing tree of Archaea: new perspectives on their diversity, evolution and ecology. *ISME J.*, **11**, 2407–2425.
3. Brochier-Armanet,C., Forterre,P. and Gribaldo,S. (2011) Phylogeny and evolution of the Archaea: one hundred genomes later. *Curr. Opin. Microbiol.*, **14**, 274–281.
4. Da Cunha,V., Gaia,M., Gadelle,D., Nasir,A. and Forterre,P. (2017) Lokiarchaea are close relatives of Euryarchaeota, not bridging the gap between prokaryotes and eukaryotes. *PLos Genet.*, **13**, e1006810.
5. Eme,L., Spang,A., Lombard,J., Stairs,C.W. and Ettema,T.J.G. (2018) Archaea and the origin of eukaryotes. *Nat. Rev. Microbiol.*, **16**, 120.
6. Koonin,E.V. (2015) Archaeal ancestors of eukaryotes: not so elusive any more. *BMC Biol.*, **13**, 84.
7. Van der Gulik,P.T.S., Hoff,W.D. and Speijer,D. (2017) In defence of the three-domains of life paradigm. *BMC Evol. Biol.*, **17**, 218.
8. Raymann,K., Brochier-Armanet,C. and Gribaldo,S. (2015) The two-domain tree of life is linked to a new root for the Archaea. *Proc. Natl. Acad. Sci. U.S.A.*, **112**, 6670–6675.
9. Yutin,N., Puigbò,P., Koonin,E.V. and Wolf,Y.I. (2012) Phylogenomics of prokaryotic ribosomal proteins. *PLoS One*, **7**, e36972.
10. Ferreira-Cerca,S. (2017) Life and death of ribosomes in archaea. In: Clouet-d'Orval,B (ed). *RNA Metabolism and Gene Expression in Archaea, Nucleic acids And Molecular Biology*. Springer International Publishing, Cham, Switzerland, Vol. **32**, pp. 129–158.
11. Werner,F. (2013) Molecular mechanisms of transcription elongation in archaea. *Chem. Rev.*, **113**, 8331–8349.
12. Fouqueau,T. and Werner,F. (2017) The architecture of transcription elongation. *Science*, **357**, 871–872.
13. Chlebowski,A., Lubas,M., Jensen,T.H. and Dziembowski,A. (2013) RNA decay machines: the exosome. *Biochim. Biophys. Acta*, **1829**, 552–560.
14. Portnoy,V. and Schuster,G. (2006) RNA polyadenylation and degradation in different Archaea; roles of the exosome and RNase R. *Nucleic Acids Res.*, **34**, 5923–5931.
15. Clouet-d'Orval,B., Batista,M., Bouvier,M., Quentin,Y., Fichant,G., Marchfelder,A. and Maier,L.-K. (2018) Insights into RNA processing pathways and associated-RNA degrading enzymes in Archaea. *FEMS Microbiol. Rev.*, **42**, 579–613.
16. Lorentzen,E., Walter,P., Fribourg,S., Evguenieva-Hackenberg,E., Klug,G. and Conti,E. (2005) The archaeal exosome core is a hexameric ring structure with three catalytic subunits. *Nat. Struct. Mol. Biol.*, **12**, 575–581.
17. Evguenieva-Hackenberg,E., Hou,L., Glaeser,S. and Klug,G. (2014) Structure and function of the archaeal exosome. *Wiley Interdiscip. Rev. RNA*, **5**, 623–635.
18. Koonin,E.V., Wolf,Y.I. and Aravind,L. (2001) Prediction of the archaeal exosome and its connections with the proteasome and the translation and transcription machineries by a comparative-genomic approach. *Genome Res.*, **11**, 240–252.
19. Hou,L., Klug,G. and Evguenieva-Hackenberg,E. (2014) Archaeal DnaG contains a conserved N-terminal RNA-binding domain and enables tailing of rRNA by the exosome. *Nucleic Acids Res.*, **42**, 12691–12706.
20. Hou,L., Klug,G. and Evguenieva-Hackenberg,E. (2013) The archaeal DnaG protein needs Csl4 for binding to the exosome and enhances its interaction with adenine-rich RNAs. *RNA Biol.*, **10**, 415–424.
21. Märtens,B., Hou,L., Amman,F., Wolfinger,M.T., Evguenieva-Hackenberg,E. and Bläsi,U. (2017) The SmAP1/2 proteins of the crenarchaeon Sulfolobus solfataricus interact with the exosome and stimulate A-rich tailing of transcripts. *Nucleic Acids Res.*, **45**, 7938–7949.
22. Evguenieva-Hackenberg,E., Roppelt,V., Finsterseifer,P. and Klug,G. (2008) Rrp4 and Csl4 are needed for efficient degradation but not for polyadenylation of synthetic and natural RNA by the archaeal exosome. *Biochemistry*, **47**, 13158–13168.
23. Witharana,C., Roppelt,V., Lochnit,G., Klug,G. and Evguenieva-Hackenberg,E. (2012) Heterogeneous complexes of the RNA exosome in Sulfolobus solfataricus. *Biochimie*, **94**, 1578–1587.
24. Dominski,Z., Carpousis,A.J. and Clouet-d'Orval,B. (2013) Emergence of the β-CASP ribonucleases: highly conserved and ubiquitous metallo-enzymes involved in messenger RNA maturation and degradation. *Biochim. Biophys. Acta*, **1829**, 532–551.
25. Condon,C. and Gilet,L. (2011) The metallo. In: *Nucelic Acids and Molecular Biology*. Springer-verlag, Berlin, Heidelberg, Vol. **26**, pp. 245–267.
26. Phung,D.K., Rinaldi,D., Langendijk-Genevaux,P.S., Quentin,Y., Carpousis,A.J. and Clouet-d'Orval,B. (2013) Archaeal β-CASP ribonucleases of the aCPSF1 family are orthologs of the eukaryal CPSF-73 factor. *Nucleic Acids Res.*, **41**, 1091–1103.
27. Clouet-d'Orval,B., Phung,D.K., Langendijk-Genevaux,P.S. and Quentin,Y. (2015) Universal RNA-degrading enzymes in Archaea: Prevalence, activities and functions of β-CASP ribonucleases. *Biochimie*, **118**, 278–285.
28. Roy,B. and Jacobson,A. (2013) The intimate relationships of mRNA decay and translation. *Trends Genet.*, **29**, 691–699.

29. Lehnik-Habrink,M., Lewis,R.J., Mäder,U. and Stülke,J. (2012) RNA degradation in Bacillus subtilis: an interplay of essential endo- and exoribonucleases. *Mol. Microbiol.*, **84**, 1005–1017.
30. Hasenöhrl,D., Lombo,T., Kaberdin,V., Londei,P. and Bläsi,U. (2008) Translation initiation factor a/eIF2(-gamma) counteracts 5′ to 3′ mRNA decay in the archaeon Sulfolobus solfataricus. *Proc. Natl. Acad. Sci. U.S.A.*, **105**, 2146–2150.
31. Märtens,B., Amman,F., Manoharadas,S., Zeichen,L., Orell,A., Albers,S.-V., Hofacker,I. and Bläsi,U. (2013) Alterations of the transcriptome of Sulfolobus acidocaldarius by exoribonuclease aCPSF2. *PLoS One*, **8**, e76569.
32. Clouet-d'Orval,B., Rinaldi,D., Quentin,Y. and Carpousis,A.J. (2010) Euryarchaeal beta-CASP proteins with homology to bacterial RNase J Have 5′- to 3′-exoribonuclease activity. *J. Biol. Chem.*, **285**, 17574–17583.
33. Hasenöhrl,D., Konrat,R. and Bläsi,U. (2011) Identification of an RNase J ortholog in Sulfolobus solfataricus: implications for 5′-to-3′ directional decay and 5′-end protection of mRNA in Crenarchaeota. *RNA*, **17**, 99–107.
34. Arkhipova,V., Stolboushkina,E., Kravchenko,O., Kljashtorny,V., Gabdulkhakov,A., Garber,M., Nikonov,S., Märtens,B., Bläsi,U. and Nikonov,O. (2015) Binding of the 5′-Triphosphate End of mRNA to the γ-Subunit of Translation Initiation Factor 2 of the Crenarchaeon Sulfolobus solfataricus. *J. Mol. Biol.*, **427**, 3086–3095.
35. Condon,C. and Putzer,H. (2002) The phylogenetic distribution of bacterial ribonucleases. *Nucleic Acids Res.*, **30**, 5339–5346.
36. Condon,C. (2010) What is the role of RNase J in mRNA turnover? *RNA Biol.*, **7**, 316–321.
37. Birien,T., Thiel,A., Henneke,G., Flament,D., Moalic,Y. and Jebbar,M. (2018) Development of an effective 6-methylpurine counterselection marker for genetic manipulation in thermococcus barophilus. *Genes (Basel)*, **9**, E77.
38. Thiel,A., Michoud,G., Moalic,Y., Flament,D. and Jebbar,M. (2014) Genetic manipulations of the hyperthermophilic piezophilic archaeon Thermococcus barophilus. *Appl. Environ. Microbiol.*, **80**, 2299–2306.
39. Pluchon,P.-F., Fouqueau,T., Crezé,C., Laurent,S., Briffotaux,J., Hogrel,G., Palud,A., Henneke,G., Godfroy,A., Hausner,W. *et al.* (2013) An extended network of genomic maintenance in the archaeon Pyrococcus abyssi highlights unexpected associations between eucaryotic homologs. *PLoS One*, **8**, e79707.
40. Branson,O.E. and Freitas,M.A. (2016) Tag-count analysis of large-scale proteomic data. *J. Proteome Res.*, **15**, 4742–4746.
41. Shannon,P., Markiel,A., Ozier,O., Baliga,N.S., Wang,J.T., Ramage,D., Amin,N., Schwikowski,B. and Ideker,T. (2003) Cytoscape: a software environment for integrated models of biomolecular interaction networks. *Genome Res.*, **13**, 2498–2504.
42. Enright,A.J., Van Dongen,S. and Ouzounis,C.A. (2002) An efficient algorithm for large-scale detection of protein families. *Nucleic Acids Res.*, **30**, 1575–1584.
43. Eddy,S.R. (2011) Accelerated profile HMM searches. *PLoS Comput. Biol.*, **7**, e1002195.
44. Edgar,R.C. (2004) MUSCLE: a multiple sequence alignment method with reduced time and space complexity. *BMC Bioinformatics*, **5**, 113.
45. Capella-Gutiérrez,S., Silla-Martínez,J.M. and Gabaldón,T. (2009) trimAl: a tool for automated alignment trimming in large-scale phylogenetic analyses. *Bioinformatics*, **25**, 1972–1973.
46. Guindon,S. and Gascuel,O. (2003) A simple, fast, and accurate algorithm to estimate large phylogenies by maximum likelihood. *Syst. Biol.*, **52**, 696–704.
47. Darriba,D., Taboada,G.L., Doallo,R. and Posada,D. (2011) ProtTest 3: fast selection of best-fit models of protein evolution. *Bioinformatics*, **27**, 1164–1165.
48. Katoh,K. and Standley,D.M. (2013) MAFFT multiple sequence alignment software version 7: improvements in performance and usability. *Mol. Biol. Evol.*, **30**, 772–780.
49. Letunic,I. and Bork,P. (2016) Interactive tree of life (iTOL) v3: an online tool for the display and annotation of phylogenetic and other trees. *Nucleic Acids Res.*, **44**, W242–W255.
50. Godfroy,A., Raven,N.D. and Sharp,R.J. (2000) Physiology and continuous culture of the hyperthermophilic deep-sea vent archaeon Pyrococcus abyssi ST549. *FEMS Microbiol. Lett.*, **186**, 127–132.
51. Omer,A.D., Ziesche,S., Ebhardt,H. and Dennis,P.P. (2002) In vitro reconstitution and activity of a C/D box methylation guide ribonucleoprotein complex. *Proc. Natl. Acad. Sci. U.S.A.*, **99**, 5289–5294.
52. Bortolin,M.-L., Bachellerie,J.-P. and Clouet-d'Orval,B. (2003) In vitro RNP assembly and methylation guide activity of an unusual box C/D RNA, cis-acting archaeal pre-tRNA(Trp). *Nucleic Acids Res.*, **31**, 6524–6535.
53. Chamieh,H., Ibrahim,H. and Kozah,J. (2016) Genome-wide identification of SF1 and SF2 helicases from archaea. *Gene*, **576**, 214–228.
54. Johnson,S.J. and Jackson,R.N. (2013) Ski2-like RNA helicase structures: common themes and complex assemblies. *RNA Biol.*, **10**, 33–43.
55. Fairman-Williams,M.E., Guenther,U.-P. and Jankowsky,E. (2010) SF1 and SF2 helicases: family matters. *Curr. Opin. Struct. Biol.*, **20**, 313–324.
56. Pyle,A.M. (2011) RNA helicases and remodeling proteins. *Curr. Opin. Chem. Biol.*, **15**, 636–642.
57. Weir,J.R., Bonneau,F., Hentschel,J. and Conti,E. (2010) Structural analysis reveals the characteristic features of Mtr4, a DExH helicase involved in nuclear RNA processing and surveillance. *Proc. Natl. Acad. Sci. U.S.A.*, **107**, 12139–12144.
58. Guy,C.P. and Bolt,E.L. (2005) Archaeal Hel308 helicase targets replication forks in vivo and in vitro and unwinds lagging strands. *Nucleic Acids Res.*, **33**, 3678–3690.
59. Fujikane,R., Komori,K., Shinagawa,H. and Ishino,Y. (2005) Identification of a novel helicase activity unwinding branched DNAs from the hyperthermophilic archaeon, Pyrococcus furiosus. *J. Biol. Chem.*, **280**, 12351–12358.
60. Li,Z., Lu,S., Hou,G., Ma,X., Sheng,D., Ni,J. and Shen,Y. (2008) Hjm/Hel308A DNA helicase from Sulfolobus tokodaii promotes replication fork regression and interacts with Hjc endonuclease in vitro. *J. Bacteriol.*, **190**, 3006–3017.
61. De Felice,M., Aria,V., Esposito,L., De Falco,M., Pucci,B., Rossi,M. and Pisani,F.M. (2007) A novel DNA helicase with strand-annealing activity from the crenarchaeon Sulfolobus solfataricus. *Biochem. J.*, **408**, 87–95.
62. Krishna,S.S., Majumdar,I. and Grishin,N.V. (2003) Structural classification of zinc fingers: survey and summary. *Nucleic Acids Res.*, **31**, 532–550.
63. Zheng,X., Feng,N., Li,D., Dong,X. and Li,J. (2017) New molecular insights into an archaeal RNase J reveal a conserved processive exoribonucleolysis mechanism of the RNase J family. *Mol. Microbiol.*, **106**, 351–366.
64. Redko,Y., Aubert,S., Stachowicz,A., Lenormand,P., Namane,A., Darfeuille,F., Thibonnier,M. and De Reuse,H. (2013) A minimal bacterial RNase J-based degradosome is associated with translating ribosomes. *Nucleic Acids Res.*, **41**, 288–301.
65. Schmidt,C., Kowalinski,E., Shanmuganathan,V., Defenouillère,Q., Braunger,K., Heuer,A., Pech,M., Namane,A., Berninghausen,O., Fromont-Racine,M. *et al.* (2016) The cryo-EM structure of a ribosome-Ski2-Ski3-Ski8 helicase complex. *Science*, **354**, 1431–1433.
66. Sharrock,W.J. and Rabinowitz,J.C. (1979) Fractionation of ribosomal particles from Bacillus subtilis. *Meth. Enzymol.*, **59**, 371–382.
67. Van Hoof,A., Staples,R.R., Baker,R.E. and Parker,R. (2000) Function of the ski4p (Csl4p) and Ski7p proteins in 3′-to-5′ degradation of mRNA. *Mol. Cell Biol.*, **20**, 8230–8243.
68. Johnson,A.W. and Kolodner,R.D. (1995) Synthetic lethality of sep1 (xrn1) ski2 and sep1 (xrn1) ski3 mutants of Saccharomyces cerevisiae is independent of killer virus and suggests a general role for these genes in translation control. *Mol. Cell Biol.*, **15**, 2719–2727.
69. Walker,J.E., Luyties,O. and Santangelo,T.J. (2017) Factor-dependent archaeal transcription termination. *Proc. Natl. Acad. Sci. U.S.A.*, **114**, E6767–E6773.
70. Maier,L.-K. and Marchfelder,A. (2019) It's all about the T: transcription termination in archaea. *Biochem. Soc. Trans.*, **47**, 461–468.
71. Rosonina,E., Kaneko,S. and Manley,J.L. (2006) Terminating the transcript: breaking up is hard to do. *Genes Dev.*, **20**, 1050–1056.
72. Sharwood,R.E., Halpert,M., Luro,S., Schuster,G. and Stern,D.B. (2011) Chloroplast RNase J compensates for inefficient transcription termination by removal of antisense RNA. *RNA*, **17**, 2165–2176.
73. Halpert,M., Liveanu,V., Glaser,F. and Schuster,G. (2019) The Arabidopsis chloroplast RNase J displays both exo- and robust endonucleolytic activities. *Plant Mol. Biol.*, **99**, 17–29.

74. Kim,K., Heo,D.-H., Kim,I., Suh,J.-Y. and Kim,M. (2016) Exosome Cofactors connect transcription termination to RNA processing by guiding terminated transcripts to the appropriate exonuclease within the nuclear exosome. *J. Biol. Chem.*, **291**, 13229–13242.
75. Jarmoskaite,I. and Russell,R. (2014) RNA helicase proteins as chaperones and remodelers. *Annu. Rev. Biochem.*, **83**, 697–725.
76. Łabno,A., Tomecki,R. and Dziembowski,A. (2016) Cytoplasmic RNA decay pathways—enzymes and mechanisms. *Biochim. Biophys. Acta*, **1863**, 3125–3147.
77. Roux,C.M., DeMuth,J.P. and Dunman,P.M. (2011) Characterization of components of the Staphylococcus aureus mRNA degradosome holoenzyme-like complex. *J. Bacteriol.*, **193**, 5520–5526.
78. Redko,Y., Galtier,E., Arnion,H., Darfeuille,F., Sismeiro,O., Coppée,J.-Y., Médigue,C., Weiman,M., Cruveiller,S. and De Reuse,H. (2016) RNase J depletion leads to massive changes in mRNA abundance in Helicobacter pylori. *RNA Biol.*, **13**, 243–253.
79. Raj,R., Mitra,S. and Gopal,B. (2018) Characterization of Staphylococcus epidermidis Polynucleotide phosphorylase and its interactions with ribonucleases RNase J1 and RNase J2. *Biochem. Biophys. Res. Commun.*, **495**, 2078–2084.
80. Tesina,P., Heckel,E., Cheng,J., Fromont-Racine,M., Buschauer,R., Kater,L., Beatrix,B., Berninghausen,O., Jacquier,A., Becker,T. *et al.* (2019) Structure of the 80S ribosome-Xrn1 nuclease complex. *Nat. Struct. Mol. Biol.*, **26**, 275–280.
81. Shoemaker,C.J. and Green,R. (2012) Translation drives mRNA quality control. *Nat. Struct. Mol. Biol.*, **19**, 594–601.
82. Doma,M.K. and Parker,R. (2006) Endonucleolytic cleavage of eukaryotic mRNAs with stalls in translation elongation. *Nature*, **440**, 561–564.
83. Parker,R. (2012) RNA degradation in Saccharomyces cerevisae. *Genetics*, **191**, 671–702.
84. Eme,L., Spang,A., Lombard,J., Stairs,C.W. and Ettema,T.J.G. (2017) Archaea and the origin of eukaryotes. *Nat. Rev. Microbiol.*, **15**, 711–723.
85. Nagarajan,V.K., Jones,C.I., Newbury,S.F. and Green,P.J. (2013) XRN 5′→3′ exoribonucleases: structure, mechanisms and functions. *Biochim. Biophys. Acta*, **1829**, 590–603.
86. Khemici,V. and Linder,P. (2018) RNA helicases in RNA decay. *Biochem. Soc. Trans.*, **46**, 163–172.
87. Redder,P. (2018) Molecular and genetic interactions of the RNA degradation machineries in Firmicute bacteria. *Wiley Interdiscip. Rev. RNA*, **9**, doi:10.1002/wrna.1460.
88. Vicens,Q., Kieft,J.S. and Rissland,O.S. (2018) Revisiting the closed-loop model and the nature of mRNA 5′-3′ communication. *Mol. Cell*, **72**, 805–812.